Visualization of nanoparticle orientation structures inside complex fluids using polarized light imaging technique

William K.A. Worby[1], Yuto Yokoyama[2], Misa Kawaguchi[1], Hiroaki Kusuno[3], Yoshiyuki Tagawa[1,*]

1: Department of Mechanical System Engineering, Tokyo University of Agriculture and Technology, Japan
2: Micro/Bio/Nanofluidics Unit, Okinawa Institute of Science and Technology Graduate University, Japan
3: Department of Mechanical Engineering, Kansai University, Japan
*Corresponding author: s240005t@st.go.tuat.ac.jp, tagawayo@cc.tuat.ac.jp

Keywords: Rheo-optics, Flow birefringence, Photoelastic method, Cellulose nanocrystal, Particle orientation.

ABSTRACT

This paper reports on the effect of three-dimensional oriented particles on birefringence introducing "Rheo-optics", one of the concepts to reveal changes in the internal structure and flow behaviour of complex fluids from changes in optical anisotropy. We applied the photoelastic method (polarization imaging technique), to a Cellulose nanocrystal (CNC) suspension under shear flow to visualize the internal orientation structure induced by the applied shear stress. For the shear flow, a rheometer that can be easily combined with a birefringence measurement system was introduced. In the experiments, birefringence was measured and compared from different directions, horizontal and vertical to the shear. According to the experimental results, the measured birefringence followed the power law of the applied shear rate with the same power exponent regardless of the direction of polarization measurements. It is also indicated that the value of the exponent is likely to vary depending on differences in the interaction behaviour between the CNCs. Furthermore, the intensity of the birefringence of the CNC suspension depended strongly on the direction of measurement relative to the shear. Specifically, birefringence in the horizontal direction of shear, i.e. the transverse rotation orientation of the CNCs, was found to be more sensitive to (shear) stress than the vertical rotation orientation.

1. Introduction

Fluids with internal structures larger than the atomic and molecular scale are called "Complex fluids" and are widely used as industrial materials. Optimising the alignment of these particles enables the production of structurally ordered soft materials with mechanical, thermal, optical and electrical properties (Håkansson et al., 2014; Thiruganasambanthan et al., 2022). However, complex fluids exhibit flow behaviour that differs significantly from that of Newtonian fluids due to changes in the internal structure caused by the flow alignment of particles in shear flow, extensional flow or combined flow. Therefore, the unravelling and understanding of the structures

induced by the flow of complex fluids is of great importance in large-scale industrial processing operations.

The theory describing the non-Brownian motion of non-spherical particles goes back to work by Jeffery (1922). Representative work by Hinch & Leal (1976) also details how Brownian motion affects the statistical distribution and rheology of axisymmetric ellipsoids, i.e. long and elongated spheres. Numerical simulations of these equations are valuable for predicting the orientation distribution and rheology of dilute suspensions of non-spherical particles. However, it still lacks good explanations for particle interactions at high concentrations. Also, the important Doi-Edwards theory (Doi & Edwards, 1978) describes the Brownian motion of high aspect ratio polymers well, yet the understanding of the dynamics of non-spherical nanoparticles in a crowded environment is incomplete. The key to the development of these particle orientation models is a reasonable characterisation of the orientation distribution and comparison with simulations.

Direct visualization of particle orientation is extremely challenging. Therefore, the particle orientation has been quantified via the degree of birefringence and dichroism in rheo-optical techniques (Rheo-optics), which clarify changes in the internal structure and flow behaviour of fluids from changes in optical anisotropy caused by the orientation of particles (Wagner, 1998; Calabrese et al., 2021). The birefringence δ_n is related to applied stress by the stress-optic law (SOL) described below (Doyle, 1982; Aben & Puro, 1997; Nakamine et al., 2024);

$$\delta_n \cos\phi = C_1(\sigma_{yy} - \sigma_{xx}) + C_2[(\sigma_{yy} + \sigma_{xx})(\sigma_{yy} - \sigma_{xx}) + {\sigma_{zy}}^2 - {\sigma_{xz}}^2], \tag{1}$$

$$\delta_n \sin\phi = 2C_1\sigma_{xy} + C_2[2(\sigma_{xx} + \sigma_{yy})\sigma_{xy} + 2\sigma_{xz}\sigma_{yz}] \tag{2}$$

Here, ϕ is the orientation angle, C_1 and C_2 are the stress-optic coefficients. Note that the z-axis is defined as the direction of the camera's optical axis (hereinafter, simply the optical axis). In previous studies, the structural and rheo-optical properties of complex fluids have been studied by applying SOL (Ito et al., 2016; Muto & Tagawa, 2022; Worby et al., 2024). However, the property measured is the anisotropy in the plane perpendicular to the optical path, providing a projected system representation. Therefore, when observing particle orientation and structural changes due to shear flow, different information is obtained depending on the direction of the observation, i.e. the direction of the light irradiation. Consequently, comparisons with eventual simulations require measurements from at least two directions for shear to obtain information on the three-dimensional (3D) orientation.

The objective of this study is to quantify the internal structural changes of complex fluids under applied stress by polarized light imaging techniques (photoelastic method). Specifically, the orientation of non-spherical particles under shear is extracted as polarization information to characterize the 3D particle orientation dynamics. As a first step, a dilute cellulose nanocrystal suspension with properties similar to Newtonian fluids, where the presence of particle-particle interactions

is small, was chosen for the study. Determining the relationship between deformation and material structure is important, and the flow provided for this purpose must be simple and controlled. In many cases, rheometers have been reported to be used to reproduce shear flow. Concentric cylinder-type (Lane et al., 2022), parallel plate-type (Hausmann et al., 2018; Worby et al., 2024) and cone plate-type (Oba & Inoue, 2016) rheometers have been reported due to their simple installation in an optical anisotropy measurement system. In the present study, we utilized two different rheometers with different measurement methods, a concentric cylinder-type and a parallel plate-type. The flow field in concentric cylinder-type rheometers, also known as Taylor-Couette flow, has no flow along the optical axis. In contrast, the latter flow field in parallel plate-type rheometers has a shear velocity distribution along the optical axis. This paper reports on the construction of rheo-optical measurement systems utilizing rheometers and a polarization camera. Based on a comparison of the birefringence measurements of each measurement system, the effect of 3D orientation on the optical anisotropy of the particles is also discussed.

2. Methodology

The present experiment used a stress-controlled rheometer (MCR302, Anton Paar Co., Ltd.) with two different measuring systems: a concentric-cylinder (CC)-type and a parallel plate (PP)-type. Unless otherwise stated, all measurements were taken at least three times and the temperature was maintained at 25°C. The shear rate applied to the suspensions was confirmed to be a condition which satisfies the limitation "Experimental window" proposed by Ewoldt et al. (2015). Therefore, the measurements described in the following section are assumed to be unaffected by surface tension or secondary flow. The details of each experimental setup are given below.

2.1. Experimental setup

2.1.1. CC-type rheometer

A schematic of the experimental setup utilizing a CC-type rheometer is shown in Fig. 1(a). In this setup, polarization measurements were conducted from a direction where there is no velocity gradient along the optical axis (horizontal to shear). The rheometer is equipped with a rotating inner cylinder (CC39, Anton Paar Co., Ltd., radius r_i = 19.4 mm, length L = 60.0 mm) and a self-constructed Taylor-Couette flow cell (A5052, radius r_o = 21.0 mm). Shear flow is induced by rotating the inner cylinder and the shear stress and torque are logged. The left-handed circularly polarized light was generated by attaching a polarizer and 1/4 wave plate to an LED light source (SOLIS-525C, Thorlabs Co., Ltd., wavelength λ = 543 nm). The circularly polarised light is reflected from the top of the inner by a mirror and emitted as elliptically polarised light with a retardation Δ. The transmitted elliptically polarised light was directed into a polarization cam-

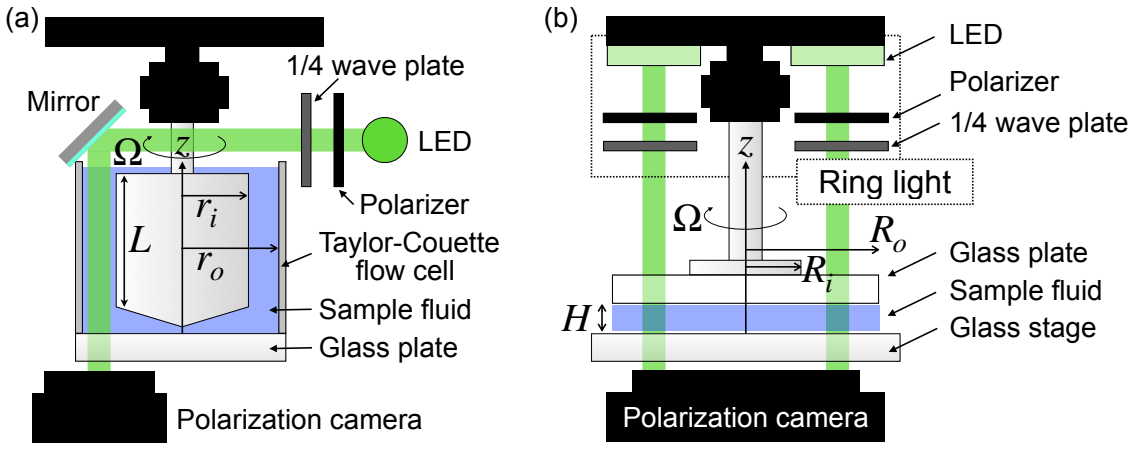

Figure 1. Schematic of rheo-optical system using (a) CC-type and (b) PP-type rheometer, where Ω is the angular velocity, L is the length of the inner cylinder, and H is the gap height, z is the coordinate axis parallel along the camera's optical axis.

era (CRYSTA PI-5WP, Photron Co., Ltd.) with a built-in 543 nm band-pass filter. The shear rate is defined from the deformation rate tensor $\mathbf{D}$ as follows:

$$\dot{\gamma} = \sqrt{2(\mathbf{D} : \mathbf{D})} = \frac{2\Omega r_o^2}{r_o^2 - {r_i}^2}, \text{where } \mathbf{D} = \frac{1}{2}(\nabla \mathbf{u} + \nabla \mathbf{u}^{\mathrm{T}}). \tag{3}$$

Here, Ω is the angular velocity and $\mathbf{u}$ is the velocity gradient tensor for the Taylor-Couette flow. In this experiment, all measurements were made at 424 pixel $\times$ 340 pixel (spatial resolution: 14 μm/pixel) and the shear rate was set to $\dot{\gamma} = 1 - 45$ s^{-1}.

2.1.2. PP-type rheometer

A schematic of the setup using a PP-type rheometer is shown in Fig. 1(b). In this setup, polarization measurements were conducted from a direction with a velocity gradient along the optical axis (vertical to shear). As with CC-type, shear flow is induced by rotating the plate and the average shear stress and torque are logged. A ring-shaped circularly polarized light source (LDR-70SE2, CCS Co., Ltd., λ = 543 nm) was mounted on the rheometer. The incident polarized light enters the polarization camera (CRYSTA PI-5WP, Photron Co., Ltd.) through the glass stage and the transparent glass plate (PP43/GL-HT, Anton Paar Co., Ltd.). All measurements were made at 424 pixel $\times$ 340 pixel (spatial resolution: 80 μm/pixel). For PP-type, the shear rate is a function of the plate radius r. We defined the shear rate by reintroducing the deformation rate tensor $\mathbf{D}$,

$$\dot{\gamma}(r) = \sqrt{2(\mathbf{D} : \mathbf{D})} = \frac{r\Omega}{H}. \tag{4}$$

H [m] is the gap height. The shear rate set on the rheometer is defined as $r = R_o$, i.e., $\dot{\gamma} = R_o\Omega/H$. Considering the requirement to satisfy the experimental window (Ewoldt et al., 2015), $\dot{\gamma} = 100 - 5300$ s^{-1} were set in the present experiments.

For more details (e.g. derivation of the deformation velocity gradient tensor) of Taylor-Couette flow and simple Couette flows in rotating parallel plates, please refer to the literature (Taylor, 1923; Schlichting & Gersten, 2016).

2.2. Polarization camera

The polarization camera (CRYSTA PI-5WP, Photron Co., Ltd., 250 fps) was used to detect the retardation Δ which is the integrated value of birefringence δ_n along the optical axis of the light transmitted through the apparatus. Based on the phase-shifting method (Onuma & Otani, 2014), Δ was obtained from the radiance through linear polarizers oriented in four different directions (0°, 45°, 90° and 135°) in an area of 2×2 pixels. Defining the light intensities detected at each of these pixels as $I_0,\ I_{90},\ I_{135}$ and I_{180} (as shown in the inset of Fig. 3(a)), Δ can be given as follows (Onuma & Otani, 2014):

$$\Delta = \int \delta_n \mathrm{d}z = \frac{\lambda}{2\pi} \sin^{-1} \frac{2\sqrt{(I_{90} - I_0)^2 + (I_{45} - I_{135})^2}}{I_0 + I_{45} + I_{90} + I_{135}}. \tag{5}$$

Here, λ [m] is the wavelength of the light source. As one Δ is calculated from 4 pixels, the spatial resolution of the Δ is $1/4$ of that of the intensity image. It is important to note that the Δ is measured as the integration of the birefringence along the optical axis. Therefore, as long as there is no stress distribution along the optical axis, or if the stress is uniformly distributed, the Δ can be calculated as the product of the birefringence δ_n and optical path length. In the present study, δ_n was calculated by simply dividing the Δ measurements by L or H.

2.3. Suspension preparation

In the present experiment, suspensions of Cellulose nanocrystals (CNC-HSFD, Cellulose Lab Ltd.) with different concentrations were studied: 0.5, 0.6 and 0.7 wt%. CNCs are rod-shaped crystals with a high aspect ratio and induce birefringence when dispersed in water (Calabrese et al., 2021; Lane et al., 2022; Worby et al., 2024) CNC suspensions were prepared by dispersing CNCs to distilled water with a stirrer (CHPS-170DF, ASONE Co., Ltd.) at 25°C, 350 rpm for 24 hours. The suspensions were then homogenized using a sonicator (UX-300, Mitsui Electric Co., Ltd.) equipped with a 12 mm probe to enhance the dispersibility. The present process was performed at 40% PWM mode for 10 minutes. The fully prepared CNC suspension's shear viscosity η was measured by rheometer with a cone plate (CP50-0.5, Anton Paar, Co., Ltd.) and is shown in Fig. 2. The absolute value of the shear viscosity increased with increasing concentration and the shear-thinning nature started to appear more strongly. Against a change in $\dot{\gamma}$ of $O(10^3)$ s^{-1}, the change in variation of η is considerably smaller as $O(0.1)$ mPa·s. In addition, the rheometer also measured the normal stress (Weizenberg effect) during the measurement, however, the values were sufficiently small to

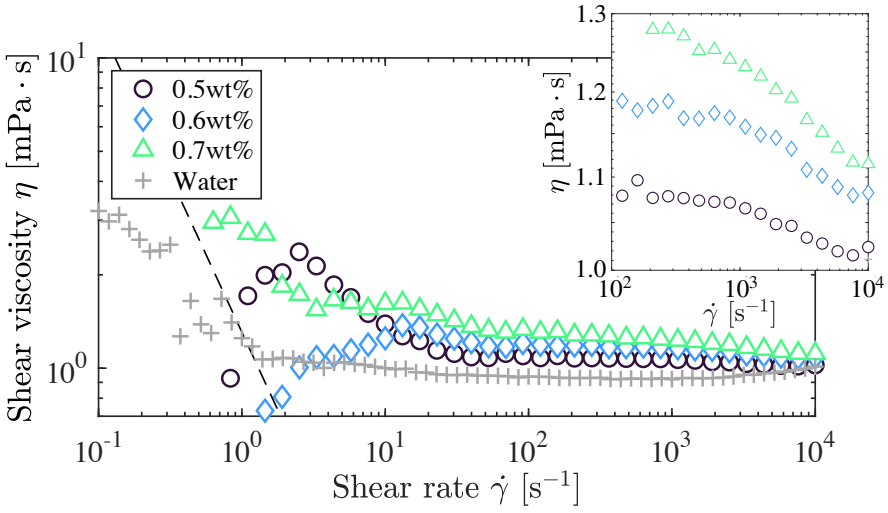

Figure 2. Steady-shear viscosity η for each CNC suspension as a function of Shear rate $\dot{\gamma}$, where the black dashed line represents the low torque limit. The inset shows the enlarged region at $10^2 - 10^4$ s^{-1}.

be regarded as a measurement error. Consequently, in the present study, CNC suspensions are regarded as a Newtonian fluid for $\dot{\gamma} > 10$ s^{-1}.

2.4. Data acquisition and analysis

The area bounded by the yellow dotted line in Fig. 3 was defined as the region of interest (hereafter, ROI). The ROI was chosen to ensure the uniformity of the lighting system, as the polarizers used the light intensity itself to calculate Δ, as described in Sec. 2.2. The software (CRYSTA Stress Viewer, Photron Co., Ltd.) was used to obtain the Δ field during the flow by background subtraction. This background-subtraction process is based on the presence of a certain degree of unevenness on the plate surface or birefringence in the plate or stage itself, which can cause a spatial distribution of retardation even when there is no flow. In addition, the concentricity or parallelism

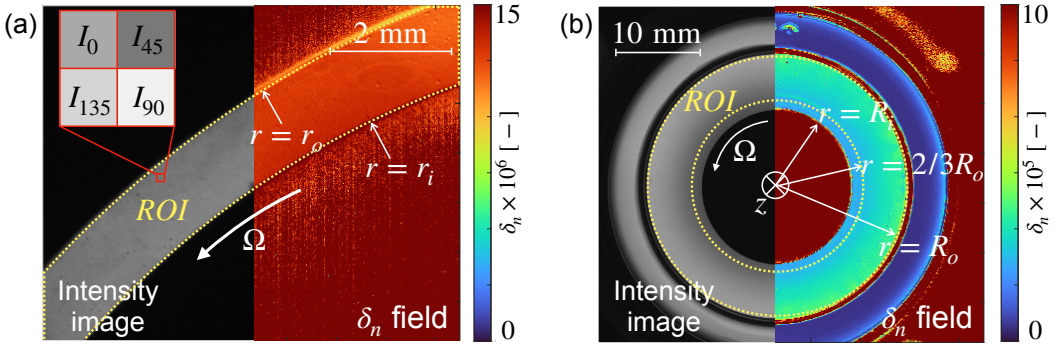

Figure 3. Representative intensity image and birefringence δ_n field for (a) CC-type and (b) PP-type setup. The areas bounded by the yellow dotted line were defined as ROI.

of the plate to the stage is not perfect, and therefore the measured Δ may also vary over time. To avoid this effect, Δ measurements were taken after a sufficient time had passed since the start of the inner cylinder or plate rotation, and 250 frames were averaged (1-second time average).

3. Results and Discussions

3.1. Characterization of birefringence

The birefringence δ_n induced in response to the shear rate in the CC and PP-type system is shown in Fig. 4. In the CC-type system (Fig. 4(a)), the birefringence δ_n increased proportionally to the shear rate, which is the same tendency as in the previous study using milling yellow suspensions (Peebles et al., 1964). However, the obtained birefringence δ_n intensity was about 1/10 of that in the previous study, where $\delta_n \sim O(10^{-6})$. Using an apparatus similar to the present CC-type system, Lane et al. (2022) reported that the birefringence intensity of CNC suspensions was $\delta_n \sim O(10^{-5})$, which is a relatively large value compared to the present results. The response sensitivity of flow alignment to shear as birefringence is considered to be caused by differences in CNC morphology. Flow birefringence has often been reported to approach a constant value at high shear rates due to the perfect alignment of the particles (Decruppe et al., 1995; Santos et al., 2023). As the experimental window limited the shear rate, the tendency of birefringence for $\dot{\gamma} > 45$ s^{-1} is uncertain, although it is expected to eventually reach a constant value as the advection forces the alignment to be further aligned (Lang et al., 2019).

The PP-type system (Fig. 4(b)) showed different trends with a threshold value of $\dot{\gamma} = 2000$ s^{-1}. For $\dot{\gamma} > 2000$ s^{-1}, it showed a tendency to increase non-linearly with the shear rate. This non-linear

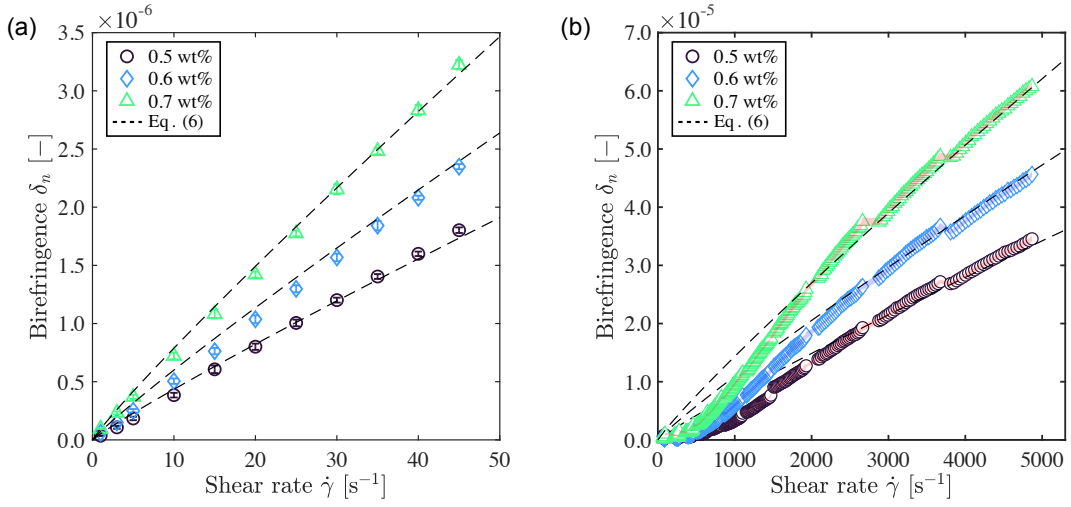

Figure 4. Measured birefringence δ_n with (a) CC-type and (b) PP-type rheometer organized by applied shear rate. Error bars and red shading indicate standard deviations. The dashed line represents the fitted Eq. (6), respectively.

increase in birefringence has also been reported for various birefringent fluids, including xanthan gum and micellar solutions (Decruppe et al., 1995; Detert et al., 2023). In addition, the obtained birefringence intensities were comparable to previous studies with $\delta_n \sim O(10^{-5})$. Meanwhile, for $\dot{\gamma} < 2000\ \mathrm{s}^{-1}$, the measurement accuracy could be low due to the resolution of the intensity values that the polarization camera image sensors can detect. We assume that the birefringence therefore temporarily exhibited a different trend for the shear rate.

As expected, the birefringence induced for the same shear rate increased with increasing concentration of CNC suspensions. The rotational diffusion coefficient of the CNCs is decreased as the suspension concentration increases (Maguire et al., 1980). This is due to the interaction of the CNCs with each other and their rotational motion being inhibited or restricted by neighbouring particles (Tao et al., 2005). Therefore, the shear rate required for CNCs to align decreases with the concentration.

Next, the trend of birefringence for the shear rate was investigated. Lane et al. (2022) proposed the following empirical equation can describe the relationship between shear rate and birefringence:

$$\delta_n = (A \cdot \dot{\gamma})^n \cdot c^m. \tag{6}$$

Here, A [s], m [–] and n [–] are fitting parameters and c [–] is suspension concentration. It should be noted that this equation may not have direct physical meaning. The experimental results were fitted using Eq. (6), and the black dash-line in Fig. 4 shows the results. The fitting parameters are shown in Table 1. Interestingly, the values of n and m are identical in both systems, while the magnitude of A differs by a factor of 10. The contribution of the different directions of polarization measurement to the shear is indicated in the fitting parameter A. In the case of simple shear flows, which have been widely studied, rod-like particles such as CNCs move along orbital trajectories known as Jeffery orbit (Jeffery, 1922). Based on this theory, CC-type systems measure the orientation of CNCs rotating in the plane perpendicular to the incident polarization, as birefringence. In contrast, the PP-type experimental system can be understood as measuring the rotating orientation of the CNCs in the plane perpendicular to the incident polarization as birefringence. Thus, differences in the magnitude of the fitting parameter A can be considered to correspond to the contribution of optical anisotropy from the direction of rotation (orientation) of the particles. The present results indicate that regardless of the direction of polarization measurement to shear, there seems to be a common physical background that leads to the flow birefringence producing

Table 1. Fitting parameters used in the present study.

	A [s]	n [–]	m [–]
CC-type	3.03×10^{-4}	0.93	1.76
PP-type	7.40×10^{-5}	0.92	1.77

a power law for the shear rate. Calabrese et al., conducted experiments with dilute CNC suspension of 0.1 wt% and reported $\delta_n \sim \dot{\gamma}^{0.9}$ (Calabrese et al., 2021). Lane et al. (2022) also provided that $\delta_n \sim \dot{\gamma}^{0.537}$ in part of an investigation into whether CNC suspensions (0.7–1.3 wt%) can be used for studies of flow birefringence. Our obtained exponents are close to the values reported by Calabrese et al. (2021), however, they differed significantly from those reported by Lane et al. (2022). Several reasons can be given for this difference, although it can be explained by differences in the interaction behaviour of the CNCs due to differences in suspension concentration and rod lengths (Maguire et al., 1980).

3.2. Calibration of stress-optic coefficient

The fitting parameter A is also considered to correspond to the sensitivity of birefringence to shear stress. Therefore, the stress-optic coefficients were calibrated using the torques logged in the CC-type and PP-type systems. The stress tensor $\sigma_{\mathbf{cc}}$ of a z-axis symmetric Taylor-Couette flow is given by using the cylindrical (rθz) coordinate system as below:

$$\sigma_{cc} = \begin{bmatrix} -P & \tau_{r\theta} & 0 \\ \tau_{\theta r} & -P & 0 \\ 0 & 0 & -P \end{bmatrix}, \text{where } \tau_{r\theta}(\tau_{\theta r}) = -\eta r \frac{\partial}{\partial r}\Big(\frac{v_\theta(r)}{r}\Big)|_{r=r_i}. \tag{7}$$

Here, v_θ is the azimuthal velocity component of the Taylor-Couette flow and P is the atmospheric pressure. Between torque T and shear stress $\tau_{r\theta}$, $T = 2\pi L {r_i}\cdot\tau_{r\theta}|_{r=r_i}$ hold, and substituting the stress components into SOL (Eqs. (1) and (2)) after transforming the coordinates to the Cartesian (xyz) coordinate system yields:

$$C_1 = \frac{\delta_n \pi}{LT} {r_i}^2. \tag{8}$$

The same assumptions can also be made in the case of the PP-type, which finally yields to

$$\sigma_{pp} = \begin{bmatrix} -P & 0 & 0 \\ 0 & -P & \tau_{\theta z} \\ 0 & \tau_{z\theta} & -P \end{bmatrix}, \text{where } \tau_{\theta z}(\tau_{z\theta}) = \eta \frac{\partial v_\theta(r,z)}{\partial z}. \tag{9}$$

$$C_2 = \frac{\delta_n}{r^2}\Big(\frac{\pi {R_o}^4}{2T}\Big)^2 \ (R_i \le r \le R_o). \tag{10}$$

Here, σ_{pp} is the stress tensor of Couette flow in the PP-type system. By substituting the torque logged by the rheometer and δ_n measurements into Eqs. (8) and (10), the stress-optic coefficients can be calibrated experimentally.

The variation of the stress-optic coefficient with shear rate is shown in Fig. 5. In Fig. 5(a), the C_1 increased with increasing shear rate for the range 1 $s^{-1} \le \dot{\gamma} \le 10$ s^{-1}. This can be the effect of the

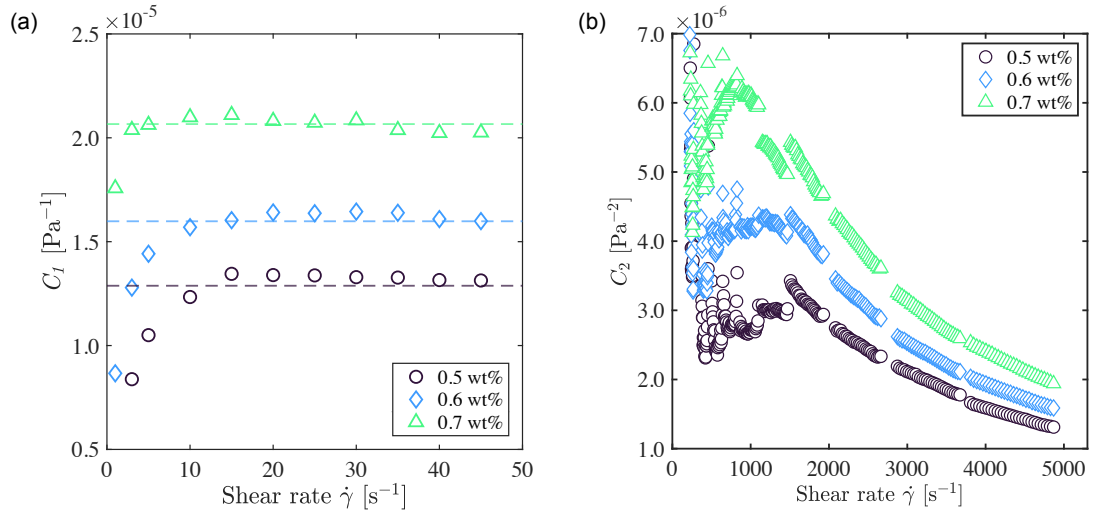

Figure 5. Calibrated stress-optic coefficients (a) C_1 and (b) C_2. The dashed line in (a) represents the average value for each suspension concentration.

non-Newtonian nature of the CNC suspension at low shear (Fig. 2). On the other hand, in the range $\dot{\gamma}$ >10 s^{-1} where the CNC suspension exhibited properties similar to Newtonian fluids, the C_1 were almost constant values. Specifically, the averaged values (dashed lined shown in Fig. 5(a)) were 1.23×10^{-5}, 1.60×10^{-5} and 2.06×10^{-5} [Pa^{-1}] at 0.5, 0.6 and 0.7 wt%, respectively. The validity of the stress-optic coefficients C_1 is discussed and compared with values reported in previous studies. C_1 is also known as the photoelastic coefficient, and although it is less reported than for solids, there are some examples of reported photoelastic coefficients for fluids. For reference, stress-optic coefficients of worm-like micellar were $O(10^{-7})$ [Pa^{-1}] (Shikata et al., 1994; Ito et al., 2016), xanthan gum solution was 3.3×10^{-8} [Pa^{-1}] (Yevlampieva et al., 1999). The particles in both fluids are of chain-like geometry, which is different from rods such as CNCs. In the case of chain-like particles, the effects of particle-particle interactions (bending, elongation and tangling) due to flexibility differ from those of CNCs. Another case study using crystalline suspensions, where the effect of particle flexibility seems to be small, is KaleidoFlow, a plate/flake vermiculite dispersion. Noto et al. (2020) estimated the stress-optic coefficient of KaleidoFlow to be 4×10^{-3} [Pa^{-1}], which is of a higher order than for CNC suspensions. The degree of particle-particle interaction also changes with different geometries, even for non-flexible crystalline suspensions. Therefore, it is considered that the difference in the effect of particle-particle interaction is one of the reasons for the difference in the order of C_1. Nakamine et al. (2024) also used CNC suspensions provided by the same supplier (Cellulose Lab. Co., Ltd.) as the CNC used in the present study, and reported $C_1 \sim 1.0 - 3.0 \times 10^{-5}$ [Pa^{-1}]. These values were close to the values of C_1 calibrated in the present experiment. From the comparison of C_1, it can be concluded that the CNC suspensions used in the present experiment, excluding KaleidoFlow, have a greater degree of optical anisotropy to applied stress than the materials covered in previous studies.

C_2 decreased as a power of the shear rate in the range $\dot{\gamma}$ >2000 s^{-1} (Fig. 5(b)). For $\dot{\gamma}$ ≤2000 s^{-1} the birefringence measurements of the polarization camera may be less accurate, as described in Sec. 3.1. Further investigation of the calibration value of C_2 in this region is necessary and is an issue to be addressed. Additionally, C_2 increased with increasing concentration of CNC suspension. This means that the sensitivity to stress (degree of optical-anisotropy) increased with increasing concentration, which is a well-known trend. However, this result infers that C_2 appears to be a physical quantity determined by the internal structure and the flow field. There have been very few reports on the C_2 of fluids and, to the best of our knowledge, this is the first systematic measurement report to identify the C_2 value of a birefringent fluid. Simple comparisons are difficult because of the different units, i.e., Pa^{-1} and Pa^{-2}, the magnitude differed from $C_1 \sim O(10^{-5})$ whether $C_2 \sim O(10^{-6})$. This indicates that the birefringence due to the transverse rotational orientation of CNCs is more sensitive to shear stress than the birefringence due to the longitudinal rotational orientation. This difference in the magnitude of the stress-optic coefficient may explain the difference in the magnitude of the fitting parameter A in Eq. (6) and could be a clue giving its physical meaning.

4. Conclusions

In the present study, the flow alignment structure of CNC suspensions under applied shear stress was visualized by introducing the concept of Rheo-optics. This study's novelty lies in quantifying the effect of the three-dimensional orientation of the CNCs on the birefringence by performing polarization measurements from different directions for shear. The birefringence followed the power law of the shear rate with the same power exponent, independent of the shear direction of the birefringent measurement. However, the proportionality coefficients differed by a factor of 10, clearly showing the difference depending on the direction of the birefringence measurement. These results suggest that there is a common physical background for birefringence to produce a power-law velocity in shear rate. In addition, this exponent differed from the values given in previous studies and is explained by differences in particle interaction behaviour depending on the suspension concentration and the length of CNCs. The stress-optic coefficients C_1 and C_2, corresponding to the first and second proportionality coefficients of the stress-optic law, were $C_1 \sim O(10^{-5})$ and $C_2 \sim O(10^{-6})$, respectively. These results indicate that the degree of optical anisotropy of the CNC suspension depends on the direction of measurement for shear, i.e. the direction of rotation of the CNCs.

Acknowledgements

This work was supported by JSPS KAKENHI Grant Nos. JP20H00222 and JP20H00223, and JST PRESTO Grant No. JPMJPR21O5.

Nomenclature

δ_n	Birefringence [–]
ϕ	Orientation angle [deg]
C_1	Stress-optic coefficient [Pa^{-1}]
C_2	Stress-optic coefficient [Pa^{-2}]
$\dot{\gamma}$	Shear rate [s^{-1}]
Ω	Angular velocity [rad/s]
L	Length of the inner cylinder [m]
r_i	Radius of the inner cylinder [m]
H	Plate gap height [m]
R_0	Radius of plate [m]
Δ	Retardation [m]
λ	Wavelength [m]
η	Steady-shear viscosity [Pa· s]

References

Aben, H., & Puro, A. (1997). Photoelastic tomography for three-dimensional flow birefringence studies. *Inverse Problems*, *13*(2), 215–221. doi: 10.1088/0266-5611/13/2/002

Calabrese, V., Haward, S. J., & Shen, A. Q. (2021). Effects of Shearing and Extensional Flows on the Alignment of Colloidal Rods. *Macromolecules*, *54*(9), 4176–4185. doi: 10.1021/acs.macromol.0c02155

Decruppe, J. P., Cressely, R., Makhloufi, R., & Cappelaere, E. (1995). Flow birefringence experiments showing a shear-banding structure in a CTAB solution. *Colloid Polym Sci*, *273*(4), 346–351. doi: 10.1007/BF00652348

Detert, M., Santos, T. P., Shen, A. Q., & Calabrese, V. (2023). Alignment–Rheology Relationship of Biosourced Rod-Like Colloids and Polymers under Flow. *Biomacromolecules*, *24*(7), 3304–3312. doi: 10.1021/acs.biomac.3c00347

Doi, M., & Edwards, S. F. (1978). Dynamics of rod-like macromolecules in concentrated solution. Part 2. *J. Chem. Soc., Faraday Trans. 2*, *74*(0), 918–932. doi: 10.1039/F29787400918

Doyle, J. F. (1982). On a nonlinearity in flow birefringence. *Experimental Mechanics*, *22*(1), 37–38. doi: 10.1007/BF02325702

Ewoldt, R. H., Johnston, M. T., & Caretta, L. M. (2015). Experimental challenges of shear rheology: How to avoid bad data. In S. E. Spagnolie (Ed.), *Complex fluids in biological systems: Experiment, theory, and computation* (pp. 207–241). New York, NY: Springer New York.

Håkansson, K. M. O., Fall, A. B., Lundell, F., Yu, S., Krywka, C., Roth, S. V., … Söderberg, L. D. (2014). Hydrodynamic alignment and assembly of nanofibrils resulting in strong cellulose filaments. *Nat Commun*, *5*(1), 4018. doi: 10.1038/ncomms5018

Hausmann, M. K., Rühs, P. A., Siqueira, G., Läuger, J., Libanori, R., Zimmermann, T., & Studart, A. R. (2018). Dynamics of Cellulose Nanocrystal Alignment during 3D Printing. *ACS Nano*, *12*(7), 6926–6937. doi: 10.1021/acsnano.8b02366

Hinch, E. J., & Leal, L. G. (1976). Constitutive equations in suspension mechanics. Part 2. Approximate forms for a suspension of rigid particles affected by Brownian rotations. *Journal of Fluid Mechanics*, *76*(1), 187–208. doi: 10.1017/S0022112076003200

Ito, M., Yoshitake, Y., & Takahashi, T. (2016). Shear-induced structure change in shear-banding of a wormlike micellar solution in concentric cylinder flow. *Journal of Rheology*, *60*(5), 1019–1029. doi: 10.1122/1.4961034

Jeffery, G. (1922). The motion of ellipsoidal particles immersed in a viscous fluid | Proceedings of the Royal Society of London. Series A, Containing Papers of a Mathematical and Physical Character. *Royal Society*, *102*(715), 161–179. doi: 10.1098/rspa.1922.0078

Lane, C., Rode, D., & Rösgen, T. (2022). Birefringent properties of aqueous cellulose nanocrystal suspensions. *Cellulose*, *29*(11), 6093–6107. doi: 10.1007/s10570-022-04646-y

Lang, C., Kohlbrecher, J., Porcar, L., Radulescu, A., Sellinghoff, K., Dhont, J. K. G., & Lettinga, M. P. (2019). Microstructural Understanding of the Length- and Stiffness-Dependent Shear Thinning in Semidilute Colloidal Rods. *Macromolecules*, *52*, 9604–9612. doi: 10.1021/acs.macromol.9b01592

Maguire, J. F., McTague, J. P., & Rondelez, F. (1980). Rotational Diffusion of Sterically Interacting Rodlike Macromolecules. *Phys. Rev. Lett.*, *45*(23), 1891–1894. doi: 10.1103/PhysRevLett.45.1891

Muto, M., & Tagawa, Y. (2022). Unsteady rheo-optical measurements of uniaxially extending liquid polymers. *arXiv*. doi: 10.48550/arXiv.2204.13450

Nakamine, K., Yokoyama, Y., Worby, W. K. A., Muto, M., & Tagawa, Y. (2024). *Flow Birefringence of Cellulose Nanocrystal Suspensions in Three-Dimensional Flow Fields: Revisiting the Stress-Optic Law* (No. arXiv:2402.16351).

Noto, D., Tasaka, Y., Hitomi, J., & Murai, Y. (2020). Applicability evaluation of the stress-optic law in Newtonian fluids toward stress field measurements. *Phys. Rev. Research*, *2*(4), 043111. doi: 10.1103/PhysRevResearch.2.043111

Oba, N., & Inoue, T. (2016). An apparatus for birefringence and extinction angle distributions measurements in cone and plate geometry by polarization imaging method. *Rheol Acta*, *55*(9), 699–708. doi: 10.1007/s00397-016-0952-5

Onuma, T., & Otani, Y. (2014). A development of two-dimensional birefringence distribution measurement system with a sampling rate of 1.3MHz. *Optics Communications*, *315*, 69–73.

Peebles, F. N., Prados, J. W., & Honeycutt Jr., E. H. (1964). Birefringent and rheologic properties of milling yellow suspensions. *Journal of Polymer Science Part C: Polymer Symposia*, *5*(1), 37–53. doi: 10.1002/polc.5070050105

Santos, T. P., Calabrese, V., Boehm, M. W., Baier, S. K., & Shen, A. Q. (2023). Flow-induced alignment of protein nanofibril dispersions. *Journal of Colloid and Interface Science*, *638*, 487–497. doi: 10.1016/j.jcis.2023.01.105

Schlichting, H., & Gersten, K. (2016). *Boundary-layer theory*. Springer Berlin Heidelberg.

Shikata, T., Dahman, S. J., & Pearson, D. S. (1994). Rheo-Optical Behavior of Wormlike Micelles. *Langmuir*, *10*(10), 3470–3476. doi: 10.1021/la00022a019

Tao, Y.-G., den Otter, W. K., Padding, J. T., Dhont, J. K. G., & Briels, W. J. (2005). Brownian dynamics simulations of the self- and collective rotational diffusion coefficients of rigid long thin rods. *The Journal of Chemical Physics*, *122*(24), 244903. doi: 10.1063/1.1940031

Taylor, G. I. (1923). Experiments on the motion of solid bodies in rotating fluids. *Philosophical Transactions of the Royal Society A*, *223*(605-615), 289–343. doi: 10.1098/rspa.1923.0103

Thiruganasambanthan, T., Ilyas, R. A., Norrrahim, M. N. F., Kumar, T. S. M., Siengchin, S., Misenan, M. S. M., … Razman, M. R. (2022). Emerging Developments on Nanocellulose as Liquid Crystals: A Biomimetic Approach. *Polymers*, *14*(8), 1546. doi: 10.3390/polym14081546

Wagner, N. J. (1998). Rheo-optics. *Current Opinion in Colloid & Interface Science*, *3*(4), 391–400. doi: 10.1016/S1359-0294(98)80055-1

Worby, W. K. A., Nakamine, K., Yokoyama, Y., Muto, M., & Tagawa, Y. (2024). *Examination of Flow Birefringence Induced by the Shear Components along the Optical Axis Using a Parallel-Plate-Type Rheometer* (No. arXiv:2405.10969).

Yevlampieva, N. P., Pavlov, G. M., & Rjumtsev, E. I. (1999). Flow birefringence of xanthan and other polysaccharide solutions. *International Journal of Biological Macromolecules*, *26*(4), 295–301. doi: 10.1016/S0141-8130(99)00096-3